Geophysical Research Letters

RESEARCH LETTER
10.1029/2020GL091520

Key Points:

- Satellite retrievals of tropospheric NO_2 and HCHO show drought enhancements of 3.5% and 7.7%, respectively, during Eastern US summers
- Low precipitation and high temperatures both independently drive HCHO drought enhancement (10%) in Southeast US woody savannas
- High temperatures drive NO_2 drought enhancement (6.0%) in Midwest US croplands and grasslands

Supporting Information:

Supporting Information may be found in the online version of this article.

Correspondence to:

J. G. Naimark and A. M. Fiore,
jgn2113@columbia.edu;
amfiore@ldeo.columbia.edu

Citation:

Naimark, J. G., Fiore, A. M., Jin, X., Wang, Y., Klovenski, E., & Braneon, C. (2021). Evaluating drought responses of surface ozone precursor proxies: Variations with land cover type, precipitation, and temperature. *Geophysical Research Letters*, *48*, e2020GL091520. https://doi.org/10.1029/2020GL091520

Received 4 NOV 2020
Accepted 5 MAR 2021

Evaluating Drought Responses of Surface Ozone Precursor Proxies: Variations With Land Cover Type, Precipitation, and Temperature

Jacob G. Naimark[1,2], Arlene M. Fiore[2], Xiaomeng Jin[3], Yuxuan Wang[4], Elizabeth Klovenski[4], and Christian Braneon[5,6]

[1]Department of Earth and Environmental Sciences, Columbia College, Columbia University, New York, NY, USA, [2]Department of Earth and Environmental Sciences, Lamont-Doherty Earth Observatory, Columbia University, Palisades, NY, USA, [3]Department of Chemistry, University of California Berkeley, Berkeley, NY, USA, [4]Department of Earth and Atmospheric Sciences, University of Houston, Houston, TX, USA, [5]NASA Goddard Institute for Space Studies (GISS), New York, NY, USA, [6]SciSpace, LLC, Bethesda, MD, USA

Abstract Prior work suggests drought exacerbates US air quality by increasing surface ozone concentrations. We analyze 2005–2015 tropospheric column concentrations of two trace gases that serve as proxies for surface ozone precursors retrieved from the OMI/Aura satellite: Nitrogen dioxide (ΩNO_2; NO_x proxy) and formaldehyde (ΩHCHO; VOC proxy). We find 3.5% and 7.7% summer drought enhancements (classified by SPEI) for ΩNO_2 and ΩHCHO, respectively, corroborating signals previously extracted from ground-level observations. When we subset by land cover type, the strongest ΩHCHO drought enhancement (10%) occurs in the woody savannas of the Southeast US. By isolating the influences of precipitation and temperature, we infer that enhanced biogenic VOC emissions in this region increase ΩHCHO independently with both high temperature and low precipitation during drought. The strongest ΩNO_2 drought enhancement (6.0%) occurs over Midwest US croplands and grasslands, which we infer to reflect the sensitivity of soil NO_x emissions to temperature.

Plain Language Summary Projected increases in drought severity and frequency for this century raise questions regarding possible impacts on air quality. Surface ozone, an air pollutant estimated to cause over 1 million annual premature deaths globally, forms when its precursor gases react in the sunlit atmosphere. These precursor gases depend on temperature and precipitation and thus can respond to drought. We analyze over a decade of satellite observations of two trace gases relevant to ozone formation and find that, on average, their concentrations increase during summer droughts in the Eastern US. While higher temperatures during droughts are usually associated with observed increases in trace gas concentrations, in the Southeast US we find increases associated with low precipitation independent of temperature. Satellite detection of these changes implies promise for application to other regions and more generally for improving mechanistic understanding of air quality responses to drought and other climate extremes.

1. Introduction

Surface ozone pollution exacerbates respiratory diseases and has been linked to 1.23 million premature fatalities across the globe annually (Lelieveld et al., 2015; Malley et al., 2017). Tropospheric ozone production occurs during oxidation of volatile organic compounds (VOCs) as they react with nitrogen oxides ($NO_x = NO + NO_2$) in the presence of sunlight, and thus peaks during the warm season at mid-latitudes (Sillman et al., 1990). Surface ozone and its precursor gases, NO_x and VOCs, have been found to increase across much of North America during drought (Wang et al., 2017). More severe US droughts are projected for the 21st century due to both lower precipitation and increased evapotranspiration as temperatures rise (Dai, 2013). Understanding how ozone precursors respond to drought is relevant for improving air quality forecasts, and satellite retrievals offer expanded observational coverage to regions lacking ground instruments.

Current satellites do not directly observe near-surface ozone concentrations but may detect drought responses of ozone precursors from space (Duncan et al., 2014; Zheng et al., 2015). We use NO_2 and HCHO as

proxies for tropospheric NO_x and biogenic VOCs (BVOCs, including isoprene and monoterpenes), respectively, the major summertime ozone precursors in the Eastern US (e.g., Zhu et al., 2016). Our satellite-based analysis complements a previous study using ground-based measurements, which found a 2%–9% increase in NO_2 and a 7%–20% increase in isoprene concentrations during drought (Wang et al., 2017). We define drought as an extended period of low precipitation anomalies, which can be exacerbated by high temperatures and increased evapotranspiration, contributing to water-stressed conditions in the soil, vegetation, and the atmosphere (Wang et al., 2017). We exploit over a decade of tropospheric column NO_2 and HCHO products (hereafter denoted as ΩNO_2 and ΩHCHO) retrieved from the Ozone Monitoring Instrument (OMI) aboard the Aura satellite to investigate the implications of drought – parsed separately for the influences of temperature and precipitation – on ozone-related gases during Eastern US summers.

Several processes could contribute to enhanced ΩNO_2 during drought (Jaeglé et al., 2005; Logan, 1983): (a) soil NO_x pulses following rainfall after an extended low precipitation anomaly, especially in grasslands and croplands (Hudman et al., 2010; Jaeglé et al., 2004; Vinken et al., 2014; Williams et al., 1988; Yienger & Levy, 1995); (b) rapid decomposition of peroxy acetyl nitrate (PAN) during high temperature-driven drought (Sillman & Samson, 1995); (c) increased lightning frequency during high temperature- and low precipitation-driven drought (Price, 2009); (d) the use of additional peaker power plants to meet high demand days during temperature-driven drought, which include plants with fewer emission controls (Abel et al., 2017); and (e) the increase of wildfires during high temperature- and low precipitation-driven drought (Delmas et al., 1995; Koppmann et al., 2005). Several processes are also expected to enhance ΩHCHO during drought: (a) temperature-sensitive leaf foliage emissions of isoprene, at least until extreme water stress and/or high temperatures suppress emissions (Abeleira & Farmer, 2017; Brilli et al., 2007; Demetillo et al., 2019; Fortunati et al., 2008; Guenther et al., 1993; Lerdau & Keller, 1997; Tawfik et al., 2012) and (b) the increase of wildfires during high temperature- and low precipitation-driven drought (Koppmann et al., 2005; Price, 2009; Singh et al., 2012). Reduced wet deposition during drought could also enhance ΩNO_2 and ΩHCHO, although we find little evidence supporting a strong role for wet deposition as shown below. If droughts are associated with more frequent clear sky conditions, then higher photolysis rates would shorten lifetimes and diminish atmospheric column concentrations. Any influence from other photochemical changes during drought (Abeleira & Farmer, 2017) will vary locally with NO_x and VOCs.

In our analysis of Eastern US summers, we primarily focus on the croplands and grasslands of the Midwest US and the woody savannas of the Southeast US, where summer emissions of NO_x and BVOCs, respectively, are expected to be highest (Guenther et al., 2000; Yienger & Levy, 1995). Soil NO_x and leaf foliage emissions of BVOCs may respond non-linearly during drought. For soil NO_x, emissions from water-stressed nitrifying bacteria are initially suppressed before an anomalously high emission pulse is triggered by precipitation (Huber et al., 2020; Hudman et al., 2012; Jaeglé et al., 2004). Soil NO_x emissions also vary nonlinearly with temperature and fertilization (Oikawa et al., 2015). For leaf foliage emissions of BVOCs like isoprene, emissions increase with temperature within a species' optimum temperature range, but temperature suppresses emissions above this range, while extreme water stress has been found to non-linearly suppress isoprene emissions (Fortunati et al., 2008; Guenther et al., 1993; Potosnak et al., 2014). The monthly temporal resolution of our satellite-based analysis cannot detect non-linear drought responses occurring over hourly or daily timescales but instead indicates temporally aggregated, regional effects of drought (Zheng et al., 2017).

2. Data and Methods

2.1. Eastern US Land Cover Type Classification

We delineate the Eastern US as 23.5°N to 49.25°N and −104°W to −62°W. We further subdivide this region into the Northeast (37.75°N to 49.25°N; −91°W to −62°W), Southeast (23.5°N to 37.75°N; −91°W to −75.5°W), and Midwest (23.5°N to 49.25°N; −104°W to −91°W). We classify land cover types using the NASA Moderate Resolution Imaging Spectrometer (MODIS) MCD12Q1 Land Cover Type product (500 × 500 m resolution; Friedl & Sulla-Menashe, 2019; Strahler et al., 1999; Text S1; Figure S1). The most abundant land cover types in each of the three sub-regions of the Eastern US are croplands and grasslands in the Midwest (71% of land area), woody savannas in the Southeast (48%), and mixed forests in the Northeast (30%; Table S1). We include croplands and grasslands in a single Midwest analysis because their mean ΩNO_2 and ΩHCHO overall drought responses are the same (differences of less than 1.0%).

2.2. OMI/Aura Satellite Retrievals

We use daily QA4ECV ΩNO_2 (available 2005–2017) and ΩHCHO (available 2005–2016) retrievals from OMI/Aura (Boersma et al., 2017; De Smedt et al., 2017; Levelt et al., 2006; Zhu et al., 2017), gridded to 0.125° × 0.125° resolution by calculating the area-weighted average, as described by Jin et al. (2020). We calculate monthly means from daily observations to reduce noise. To eliminate the influence of small sample sizes, we require at least 10 valid daily measurements to calculate monthly means (Text S2; Figures S2 and S3). We compare drought versus normal conditions in June, July, and August.

2.3. Three Climate Indices: SPEI, SPI, STI

We quantify drought conditions using three climate indices; the Standardized Precipitation Evapotranspiration Index (SPEI), the Standardized Precipitation Index (SPI), and the Standardized Temperature Index (STI), which we develop by adapting the statistical approach used to generate SPI but replacing precipitation with temperature (Fan & van den Dool, 2008; McKee et al., 1993; Zscheischler et al., 2014; Text S3). Below, we often refer to SPEI as the "overall" drought index, while we parse overall drought into "P-driven" drought using SPI and "T-driven" drought using STI.

SPEI, SPI, and STI quantify climate anomalies on a monthly timescale, relative to long-term average conditions at each grid cell. SPEI (0.5° × 0.5° resolution) uses precipitation and evapotranspiration data to classify drought, which effectively incorporates both precipitation and temperature into the index. We use the SPEIbase version 2.5 dataset, which incorporates Climate Research Unit Time Series (CRU TS) precipitation and potential evapotranspiration data (University of East Anglia Climatic Research Unit et al., 2017). SPEIbase data are available through 2015 (University of East Anglia Climatic Research Unit et al., 2017; Vicente-Serrano, Beguería, & López-Moreno, 2010; Vicente-Serrano, Beguería, López-Moreno, Angulo, & El Kenawy, 2010), so we restrict drought versus normal analyses to the time period 2005–2015.

SPI incorporates only precipitation data, which makes it simpler to calculate than SPEI, but less indicative of temperature conditions (Keyantash & National Center for Atmospheric Research Staff, 2018; McKee et al., 1993; Text S3). We calculate SPI using CRU TS monthly precipitation data interpolated onto a 0.5° × 0.5° resolution grid (University of East Anglia Climatic Research Unit et al., 2020). Similarly, STI incorporates only temperature data, using monthly temperature data from the Global Historical Climatology Network and the Climate Anomaly Monitoring System (GHCN + CAMS) interpolated onto a 0.5° × 0.5° resolution grid (Fan & van den Dool, 2008; Text S3).

SPEI, SPI, and STI (0.5° × 0.5°) are converted to match the spatial resolution of the OMI/Aura data (0.125° × 0.125°) by sampling the coarser, original grid cell values that encompass each finer grid cell. MODIS (500 × 500 m) data are also re-gridded to 0.125° × 0.125° by sampling the value at the center of each coarser grid cell.

All three climate indices provide location-specific, calendar month-specific deviation values, with a mean of 0 and a standard deviation of 1, enabling comparisons across space and time. We define overall drought conditions as the 10% driest months (SPEI < -1.3) over the full 115-year record (1901–2015) from which SPEI is derived, as in Wang et al. (2017) (see Figure S4 for summer overall drought plots by year). For P-driven drought, we consider the 10% lowest precipitation months (SPI < -1.3) over the 1901–2018 period with CRU TS measurements available. For T-driven drought, we consider the 10% highest temperature months (STI > 1.3) relative to the 1948–2019 period with GHCN + CAMS measurements available. Additionally, for months to be classified as either P-driven drought or T-driven drought, they must also co-occur with overall drought conditions (defined by the overlap of SPI < -1.3 or STI >1.3 with SPEI < -1.3). We control P-driven and T-driven drought for the other variable to minimize bias in one index due to extreme values in the other. For all analyses, we include only SPI monthly values that correspond with the condition $-1.3 \leq$ STI ≤ 1.3, and we only include STI values for which $-1.3 \leq$ SPI ≤ 1.3. Non-drought (or "normal") months are defined as months with SPEI values between −0.5 and 0.5 (Wang et al., 2017).

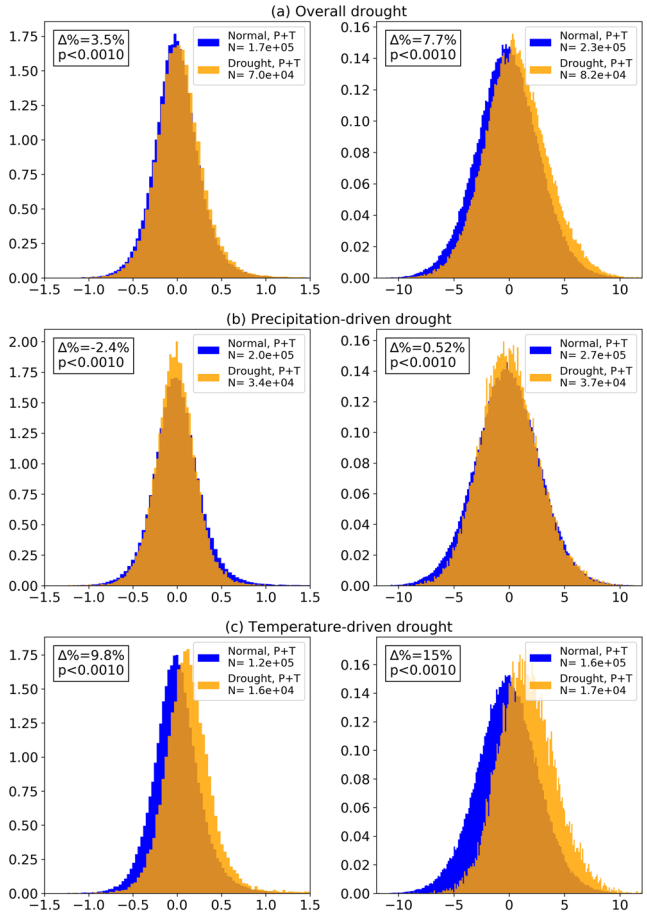

Figure 1. Probability distributions of monthly mean ΩNO_2 (left) and ΩHCHO (right) anomalies over the Eastern US during June, July, and August, separately for drought (orange) and normal (blue) conditions, where drought is defined as overall drought (a), precipitation-driven drought (b), and temperature-driven drought (c), for 2005–2015. Δ% values represent concentration percentage changes from normal to drought conditions. See Section 2.3 for definitions.

2.4. Statistical Methods

We apply Welch's t-test to assess significance in mean column concentration differences between normal and drought conditions in an attempt to account for unequal variances and sizes of our samples, assuming the underlying populations are normally distributed (Figure 1). When using Welch's t-test to compare overall drought and normal month column concentrations, we include only grid cells that experience at least three drought months and at least three normal months in order to ensure spatial consistency between the two population samples, given that normal months occur more frequently (Text S4; Figure S5). When analyzing P-driven and T-driven drought in comparison with normal conditions, we use a minimum threshold of one drought and one normal month to maximize the use of available data.

We apply ordinary (Pearson) least-squares linear regressions to understand the correlative relationship between gas concentrations and SPEI, as well as SPI and STI (each controlled for the other index, as described in Section 2.3). Despite known non-linear drought responses of NO_X and BVOCs that occur on hourly and daily timescales, the monthly linear regressions capture temporally aggregated, regional drought responses. Because linear regressions do not rely on categorical distinctions between drought and normal months, as in the case of Welch's t-test comparisons, we include all data. When we apply linear regressions to ΩNO_2 and ΩHCHO against SPI and STI, as well as to SPI against STI, we use the full period of 2005–2016 (for all ΩHCHO analyses) and 2005–2017 (for all ΩNO_2 and STI vs. SPI analyses) to maximize the OMI/Aura sample size.

3. Results & Discussion

3.1. Response of ΩHCHO and ΩNO_2 to Drought Over the Eastern US

In our broad analysis of Eastern US summers (JJA), we find a mean overall drought enhancement of 3.5% ($p < 0.0010$) in ΩNO_2 and 7.7% ($p < 0.0010$) in ΩHCHO, consistent in sign and magnitude with previous ground-level measurements of NO_x and VOCs in North America (Wang et al., 2017; Figure 1a). ΩNO_2 increases on average by 9.8% ($p < 0.0010$) during T-driven drought but changes by −2.4% ($p < 0.0010$) for P-driven drought (Figures 1b and 1c). Similarly, ΩHCHO is enhanced by 15% ($p < 0.0010$) during T-driven drought but changes little during P-driven drought (+0.52%; $p < 0.0010$; Figures 1b and 1c). We thus infer that high temperatures, rather than low precipitation, dominate the broad scale drought emissions response in the Eastern US. Given the smaller responses to precipitation than temperature, and that wet deposition is a minor HCHO sink relative to photochemical loss, we infer that changes in the wet depositional sink are not the primary driver of the regional Eastern US ΩHCHO and ΩNO_2 enhancements during drought (Tost et al., 2007). However, in the Southeast US, a decrease in a wet deposition during P-driven drought may contribute to ΩHCHO enhancements (Fried et al., 2016; Tost et al., 2007). Lastly, we cannot rule out that the small change in ΩHCHO during P-driven drought is caused by two opposite signals canceling each other out, with long term water stress simultaneously suppressing BVOC emissions and decreasing the wet depositional sink (Brilli et al., 2007; Tost et al., 2007).

The correlation between both ΩNO_2 and ΩHCHO anomalies with the temperature index, STI, in the Eastern US is stronger when we subset our data for overall drought months (SPEI < −1.3; Figure S4) than when no drought condition is applied. During overall drought, ΩNO_2 anomalies correlate positively with STI ($r = 0.21$, slope = 0.13, intercept = −0.12, $p < 0.0010$; not shown), while when ΩNO_2 anomalies are regressed against STI irrespective of SPEI (overall drought conditions), the correlation weakens ($r = 0.15$,

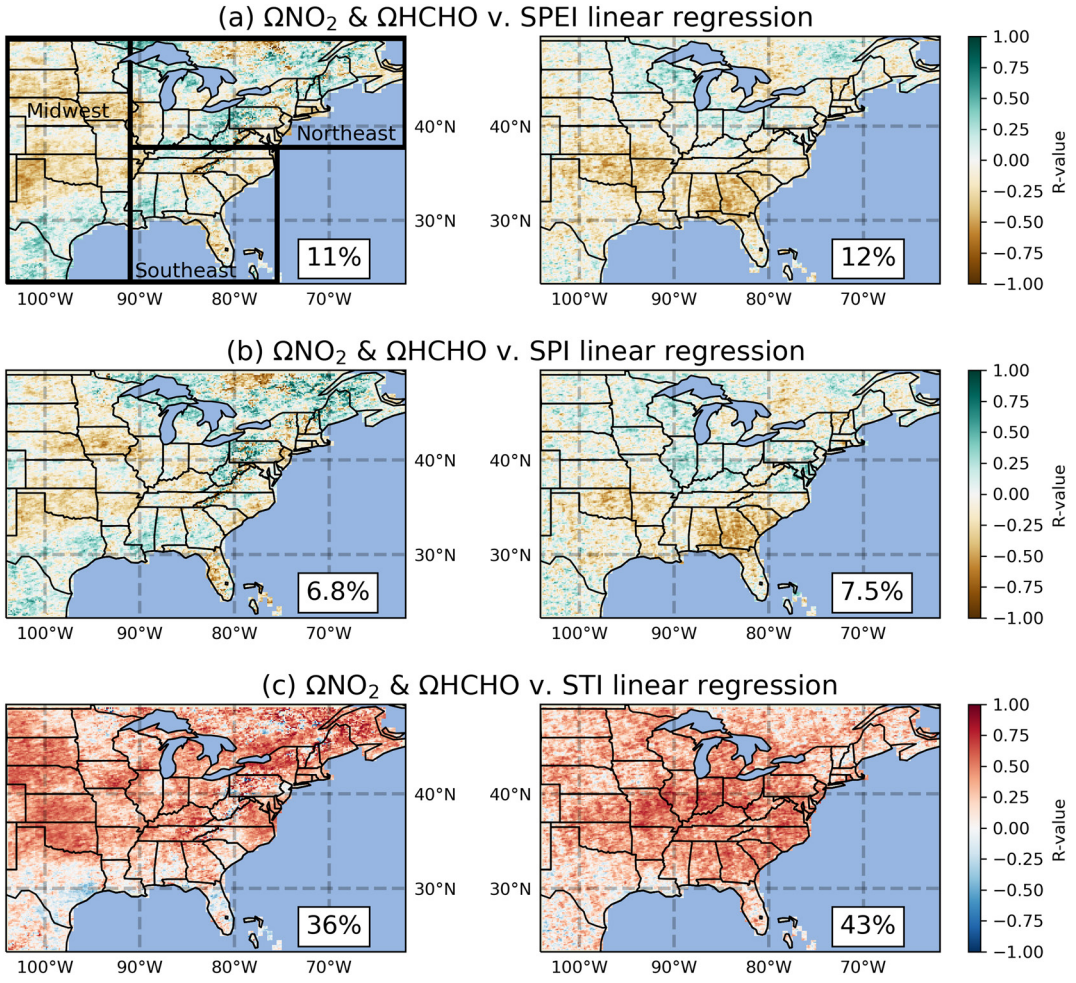

Figure 2. Ordinary least squares (Pearson) correlation of either ΩNO_2 (left) or ΩHCHO (right) monthly anomalies regressed against SPEI (top, 2a), SPI (middle, 2b), or STI (bottom, 2c) climate indices, over the Eastern US during summer (JJA). SPEI regressions (2a) are for 2005–2015, while SPI (2b) and STI (2c) regressions are for 2005–2016 (ΩHCHO) and 2005–2017 (ΩNO_2). Percentage values in the bottom, right corners show the percentage of non-water grid cells in which $p < 0.05$.

slope = 0.11, intercept = −0.093, $p < 0.0010$; not shown). Similarly, ΩHCHO anomalies correlate more strongly with STI during overall drought ($r = 0.25$; slope = 1.4; intercept = −1.0; $p < 0.0010$; not shown) than when no drought condition is applied ($r = 0.21$; slope = 1.3; intercept = −1.1; $p < 0.0010$; not shown). Each regression is applied only to the range STI > 1.3 to focus the analysis on the 10% highest temperature months comprising T-driven droughts. Given the strong temperature-dependence of ΩNO_2 and ΩHCHO sources (see Section 1), we infer that on a broad scale the sensitivity of these sources to temperature is strengthened during drought and contributes to the column enhancements, although we cannot rule out a role for decreasing sinks during drought.

3.2. Drought Response by Land Cover Type

Temporal correlations of ΩNO_2 and ΩHCHO with SPEI, SPI, or STI for individual grid cells vary regionally in the Eastern US (Figures 2a and 2c), though both ΩNO_2 and ΩHCHO have a positive correlation with STI across nearly the entire Eastern US. Because of the infrequency of drought from 2005 to 2015 in the Northeast US (Figure S5), we find only 11% (for NO_2; not shown) and 24% (for HCHO; not shown) of Northeast mixed forests grid cells are represented in our analyses after applying the minimum requirement for the number of drought and normal months (see Section 2.4). In the Midwest croplands and grasslands, 46% of

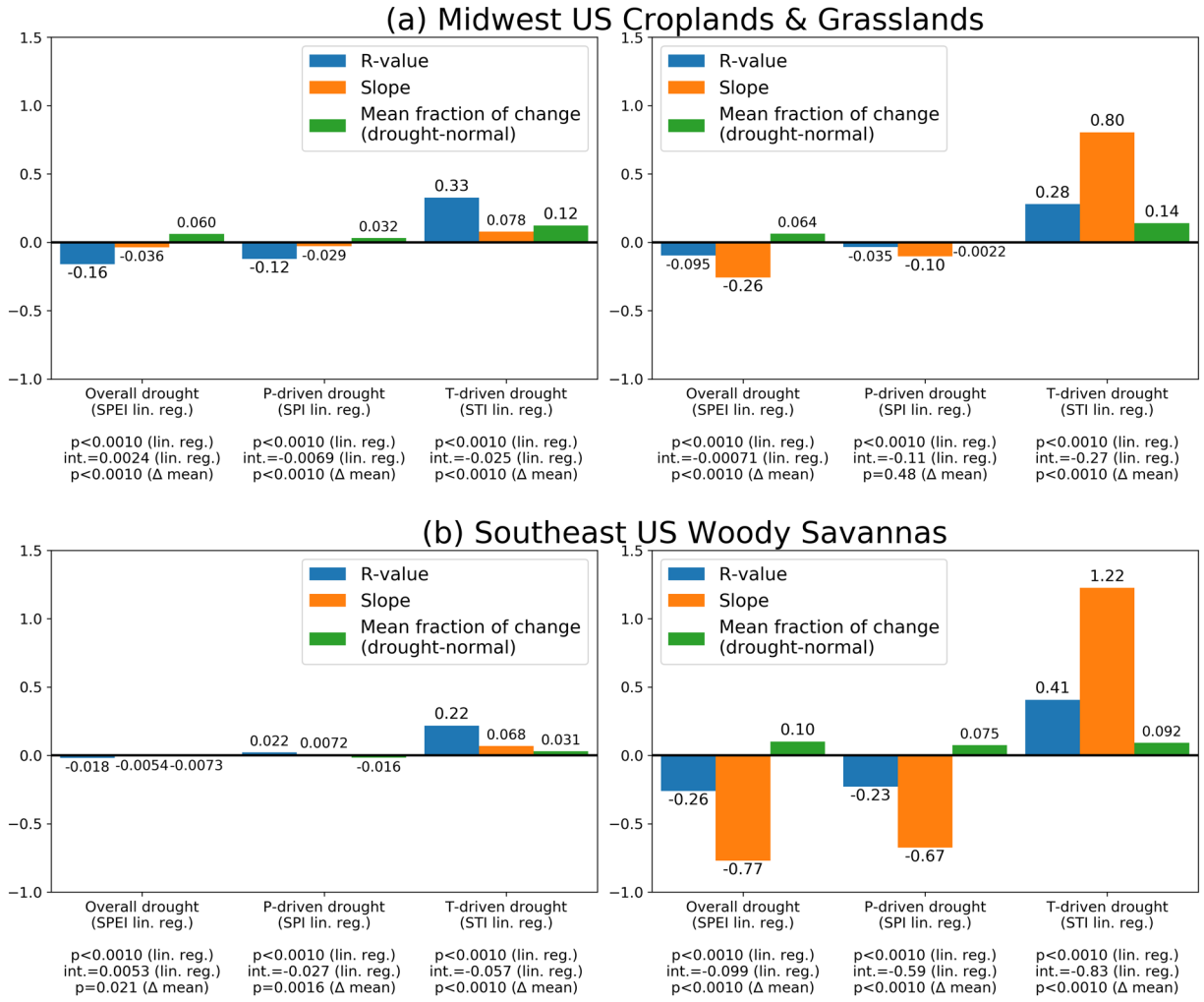

Figure 3. Midwest US croplands and grasslands (3a) and Southeast US woody savannas (3b), drought versus normal conditions comparison. ΩNO_2 (left) and ΩHCHO (right) anomalies in the region are regressed against SPEI, SPI (with the condition $-1.3 \leq STI \leq 1.3$), and STI (with the condition $-1.3 \leq SPI \leq 1.3$) for all points, with *r*-values (leftmost, blue bars), slopes (middle, orange bars) and *p*-values and intercepts reported on *x*-axis tick labels (lin. reg.). SPEI regressions are for 2005–2015, while SPI and STI regressions are for 2005–2016 (ΩHCHO) and for 2005–2017 (ΩNO_2). Mean ΩNO_2 and ΩHCHO changes between drought versus normal conditions for overall, P-driven and T-driven drought (all 2005–2015), are reported as fractions (rightmost, green bars), with *p*-values reported on *x*-axis tick labels (Δ mean).

grid cells are represented in our analyses (for both NO_2 and HCHO), while in the Southeast woody savannas 62% (for NO_2) and 75% (for HCHO) of grid cells are represented (not shown). Given the limited spatial representation of data in the Northeast mixed forests, we include findings for this region only in Figure S6, as our sample size limits us from drawing robust inferences.

ΩNO_2 is most strongly enhanced during drought in the croplands and grasslands of the Midwest US, with a mean enhancement of 6.0% ($p < 0.0010$; Figure 3a). For ΩHCHO, the strongest overall drought enhancement occurs in the woody savannas of the Southeast US, with a mean enhancement of 10% ($p < 0.0010$; Figure 3b). Because anthropogenic sources of VOCs contribute only 12% of summer VOC emissions in North America and most anthropogenic sources of VOCs and NO_x are less sensitive to climate than are natural sources, we infer that sub-regional differences in drought responses are primarily due to variation in natural (biogenic) emissions (Chen et al., 2019; Wang et al., 2017).

3.2.1. ΩNO_2

The strong overall ΩNO_2 drought enhancement (6.0%; $p < 0.0010$) in the croplands and grasslands of the Midwest mainly reflects a T-driven drought response (+12%; $p < 0.0010$), rather than a P-driven drought

response (+3.2%; $p < 0.0010$; Figure 3a). We infer that this overall ΩNO_2 drought enhancement, as well as the positive correlation between ΩNO_2 anomalies and STI ($r = 0.33$; slope = 0.078; intercept = −0.025; $p < 0.0010$) in the Midwest (Figure 3a) reflects temperature-dependent NO_x sources, such as soil NO_x, lightning, fossil fuel combustion, and/or a shorter lifetime of thermally-sensitive NO_x reservoir species, notably PAN (Abel et al., 2017; Price, 1993; Sillman & Samson, 1995; Yienger & Levy, 1995). Soil NO_x is likely the most important driver in light of earlier work indicating a strong, temperature-dependent soil NO_x signal in ΩNO_2 (Hudman et al., 2010; Vinken et al., 2014).

Despite previous findings of soil NO_x emissions pulses following rainfall on water-stressed soil (Hudman et al., 2010; Jaeglé et al., 2004; Williams et al., 1988; Yienger & Levy, 1995), we find only moderate concentration increases during P-driven drought (+3.2%; Figure 3a). Consistent irrigation could potentially explain the diminished effects of rain-pulsing emissions, as it prevents the water-stressed conditions that trigger rain-pulsing events (Oikawa et al., 2015; Yienger & Levy, 1995). Even in the absence of rain-pulsing, however, soil NO_x emissions are strongly temperature-dependent, increasing exponentially with temperature in water-saturated soils and roughly linearly in water-stressed soils, and can account for a majority of summer NO_x emissions in croplands and grasslands (Stocker et al., 1993; Yienger & Levy, 1995).

Overall, we find that ΩNO_2 increases during drought in areas where soil NO_x emissions comprise a large portion of the total emissions inventory, such as croplands and grasslands (Figure 3a; Vinken et al., 2014; Weng et al., 2020; Williams & Fehsenfeld, 1991). Consistent with this conclusion, the woody savannas of the Southeast US, where soil NO_x emissions may be 50 times smaller than in Midwest grasslands (Weng et al., 2020; Williams & Fehsenfeld, 1991), show little change in ΩNO_2 during overall drought (−0.73%; $p = 0.021$), as well as during P-driven (−1.6%; $p = 0.0016$) and T-driven drought (3.1%; $p < 0.0010$; Figure 3b).

3.2.2. ΩHCHO

The strong ΩHCHO overall drought enhancement in the Southeast US woody savannas (+10%; $p < 0.0010$) reflects both a P-driven (+7.5%; $p < 0.0010$) and T-driven drought response (+9.2%; $p < 0.0010$; Figure 3b). Previous findings have established that isoprene emissions, which account for roughly 35% of total BVOC emissions in North America, are enhanced by higher temperatures (Brilli et al., 2007; Guenther et al., 1993, 1995, 2000). Thus, we infer that the temperature response of BVOC emissions from terrestrial vegetation contributes to the positive correlation between ΩHCHO anomalies and STI values ($r = 0.41$, slope = 1.2, intercept = −0.83; $p < 0.0010$) and the negative correlation between ΩHCHO anomalies and overall drought index values ($r = -0.26$; slope = −0.77; intercept = −0.099; $p < 0.0010$; Figure 3b).

Prior work suggests extreme water-stress during P-driven drought decreases emissions (Brilli et al., 2007; Fortunati et al., 2008). We find, however, higher ΩHCHO during P-driven drought in Southeast US woody savannas (+7.5%; $p < 0.0010$; Figure 3b), in conflict with earlier work demonstrating a drying effect of low precipitation on soil moisture that decreases isoprene emissions by up to 25% during moderate water stress and up to 100% when soils are completely water-stressed (Brilli et al., 2007; Fortunati et al., 2008). While there is a weak tendency for temperatures to be higher during low precipitation months ($r = -0.21$; slope = −0.15; intercept = 0.23; $p < 0.0010$; Figure S7), this coupled influence is unlikely the dominant factor contributing to the observed 7.5% ΩHCHO enhancement (Fortunati et al., 2008).

An alternative explanation is that higher emissions of monoterpenes, another BVOC, explain the ΩHCHO enhancement during P-driven drought. Monoterpenes are known to be enhanced in water-stressed soils and are about one-third as abundant as isoprene during Southeast US summers (Hagerman et al., 1997; Ormeño et al., 2007). Monoterpenes are emitted from certain species at equally high or higher rates during water stress than during average conditions, reflecting heightened carbon use for protection from environmental stressors, such as plant decomposition and insect infestation (Guenther et al., 1995; Ormeño et al., 2007; Pfister et al., 2008; Turtola et al., 2003). During P-driven drought, monoterpenes increase by nearly 40% in some coniferous species to protect trees from these threats (Turtola et al., 2003). The lack of a similar relationship in the Midwest is consistent with our inference that monoterpene emissions contribute to the observed ΩHCHO enhancement during P-driven drought in the Southeast, as Geron et al. (2000) found that monoterpene emission fluxes in the Southeast are 3.6–20 times stronger than in the Northern and Southern Great Plains.

Additionally, during the onset of drought, water-deficient soil and air can increase leaf temperature and decrease CO_2 concentrations in forest foliage as stomatal conductance and transpiration decline (Pegoraro et al., 2005; Potosnak et al., 2014; Zhang & Wang, 2016). While long term water stress suppresses isoprene emissions (due to decreased expression of isoprene synthase), short-term water stress has been found to enhance isoprene emissions at the forest level, including in the Southeast (Fortunati et al., 2008; Pegoraro et al., 2005; Potosnak et al., 2014; Zhang & Wang, 2016). Thus, we infer that the unexpected, but substantial enhancement of ΩHCHO during P-driven drought in the Southeast reflects a yet unknown combination of monoterpene emissions from coniferous vegetation and enhanced isoprene emissions during short term and/or early drought (Brilli et al., 2007; Demetillo et al., 2019; Guenther et al., 1994; Hagerman et al., 1997; Pegoraro et al., 2005; Purves et al., 2004; Tawfik et al., 2012).

HCHO emissions from wildfires during drought could also explain a portion of the Southeast US P-driven drought enhancement (Koppmann et al., 2005; Singh et al., 2012). Assuming cloud cover changes little or declines during drought, HCHO photolysis rates are unlikely to decrease. Drier conditions, however, could reduce the loss of HCHO by reaction with the hydroxyl radical (OH) if OH production rates are limited by water vapor abundance (rather than radiation for photolysis). A decrease in OH production, however, would also reduce the chemical production of HCHO (which occurs via reaction of VOC with OH), yielding little net change in ΩHCHO (e.g., Valin et al., 2016; Zheng et al., 2017). Drought-induced changes in the balance of NO_x and VOC availability could also alter OH, though the sign of the OH response will vary locally with this NO_x-to-VOC balance.

The drought response of ΩHCHO in Midwest US croplands and grasslands is entirely dominated by T-driven drought (+14%; $p < 0.0010$) with no response during P-driven drought ($p = 0.48$), and an overall drought enhancement in Midwest croplands and grasslands of +6.4% ($p < 0.0010$; Figure 3a). These enhancements are consistent with BVOC responses, especially isoprene emissions from terrestrial vegetation in croplands and grasslands (where monoterpenes are expected to contribute little to the overall VOC budget) under warmer temperatures (Bai et al., 2006; Guenther et al., 1995). We infer that the lack of a significant ΩHCHO response to P-driven drought reflects the upward effect of higher temperatures balancing the downward effect of low precipitation on isoprene emissions, given the observed negative correlation between SPI and STI ($r = -0.29$; slope $= -0.21$; intercept $= 0.21$; $p < 0.0010$; Figure S7; Fortunati et al., 2008).

Across our study domain, photolysis is a major loss pathway for HCHO. Photolysis is expected to increase during periods with fewer clouds, like drought, intensifying the chemical loss pathway for HCHO (Matthijsen et al., 1998). As such, HCHO emission enhancements during drought may be even stronger than suggested by observed concentration enhancements if higher photolysis shortens the HCHO lifetime during drought.

4. Conclusions

The OMI/Aura satellite detects broad scale enhancements in ΩNO_2 and ΩHCHO in the Eastern US that are consistent with a previous analysis of ground-based observations in both sign and magnitude (Wang et al., 2017). NO_2 and HCHO drought enhancements are both driven more strongly by high temperatures than by low precipitation. We infer that temperature-driven enhancements reflect known emission responses to temperature that are strengthened during drought in the Eastern US.

On finer scales, we find that changes in ΩNO_2 and ΩHCHO depend on the land cover type over which drought occurs and the extent to which the drought is P-driven versus T-driven. ΩHCHO shows the largest overall drought enhancement in the woody savannas of the Southeast, with a mean enhancement of 10%. This response occurs during both P-driven and T-driven droughts, suggesting that biogenic VOC emissions from terrestrial vegetation can be enhanced even when water stress is unrelated to the influence of high temperature (Guenther et al., 1993; Ormeño et al., 2007; Pegoraro et al., 2005; Potosnak et al., 2014; Turtola et al., 2003; Zhang & Wang, 2016). We hypothesize that the increase detected in the satellite HCHO product reflects enhanced monoterpene emissions during P-driven drought, with some contribution possible from enhanced isoprene emissions during the onset of drought; this hypothesis could readily be tested with field process studies under drought versus normal conditions.

The ΩNO_2 drought enhancement is largest over Midwest croplands and grasslands, with a mean enhancement of 6.0%. We infer that soil NO_x emissions are predominantly enhanced by T-driven droughts, while surprisingly, the influence of rain pulsing during P-driven droughts does not significantly enhance column concentrations (Hudman et al., 2010; Vinken et al., 2014; Yienger & Levy, 1995). Our analysis cannot definitively distinguish the contributions of individual sources or sinks, but future work with models and higher resolution satellite data (e.g., Tropospheric Monitoring Instrument, the upcoming Tropospheric Emissions: Monitoring of Pollution [Zoogman et al., 2017; Fletcher & McMullan, 2016]) should allow for stronger constraints on source attribution.

The predicted increase in drought frequency and severity across large regions of the world in the coming century, including the Eastern US, underlines the importance of understanding the effects of drought on air pollution (Dai, 2013). Our use of satellite instruments to detect surface ozone precursor proxy gases could be extended globally to examine the mechanisms driving how pollutants, such as surface ozone, respond to climate extremes like drought.

Data Availability Statement

All data and code are archived with Columbia University Academic Commons: https://doi.org/10.7916/d8-vbrp-9034.

Acknowledgments
JGN acknowledges Dr. Martin Stute and Dr. Park Williams for contributions to early drafts and SPI MATLAB code, respectively. AMF acknowledges NASA HAQAST NNX16AQ20G and the Vetlesen Foundation; This is LDEO Contribution #8481. XJ acknowledges NASA Earth and Space Science Fellowship (NESSF, Grant 80NSSC18K1399). YW acknowledges NASA ACCMAP 80NSSC19K0986.

References

Abel, D., Holloway, T., Kladar, R. M., Meier, P., Ahl, D., Harkey, M., & Patz, J. (2017). Response of power plant emissions to ambient temperature in the eastern United States. *Environmental Science & Technology*, *51*(10), 5838–5846. https://doi.org/10.1021/acs.est.6b06201

Abeleira, A. J., & Farmer, D. K. (2017). Summer ozone in the northern Front Range metropolitan area: Weekend–weekday effects, temperature dependences, and the impact of drought. *Atmospheric Chemistry and Physics*, *17*, 6517–6529. https://doi.org/10.5194/acp-17-6517-2017

Bai, J., Baker, B., Liang, B., Greenberg, J., & Guenther, A. (2006). Isoprene and monoterpene emissions from an Inner Mongolia grassland. *Atmospheric Environment*, *40*(30), 5753–5758. https://doi.org/10.1016/j.atmosenv.2006.05.019

Boersma, F., Eskes, H., Richter, A., De Smedt, I., Lorente, A., Beirle, S., et al. (2017). *QA4ECV NO2 tropospheric and stratospheric column data from OMI*. Royal Netherlands Meteorological Institute (KNMI) Version 1.1 [Data set]. http://doi.org/10.21944/qa4ecv-no2-gome2a-v1.1

Brilli, F., Barta, C., Fortunati, A., Lerdau, M., Loreto, F., & Centritto, M. (2007). Response of isoprene emission and carbon metabolism to drought in white poplar (Populus alba) saplings. *New Phytologist*, *175*, 244–254. https://doi.org/10.1111/j.1469-8137.2007.02094.x

Chen, X., Millet, D. B., Singh, H. B., Wisthaler, A., Apel, E. C., Atlas, E. L., et al. (2019). On the sources and sinks of atmospheric VOCs: An integrated analysis of recent aircraft campaigns over North America. *Atmospheric Chemistry and Physics*, *19*(14), 9097–9123. https://doi.org/10.5194/acp-19-9097-2019

Dai, A. (2013). Increasing drought under global warming in observations and models. *Nature Climate Change*, *3*, 52–28. https://doi.org/10.1038/nclimate1633

Delmas, R., Lacaux, J. P., Menaut, J. C., Abbadie, L., Le Roux, X., Helas, G., & Lobert, J. (1995). Nitrogen compound emission from biomass burning in tropical African savanna FOS/DECAFE 1991 experiment (Lamto, Ivory Coast). *Journal of Atmospheric Chemistry*, *22*, 175–193. https://doi.org/10.1007/bf00708188

Demetillo, M. A. G., Anderson, J. F., Geddes, J. A., Yang, X., Najacht, E. Y., Herrera, S. A., et al. (2019). Observing Severe Drought Influences on Ozone Air Pollution in California. *Environmental Science & Technology*, *53*(9), 4695–4706. https://doi.org/10.1021/acs.est.8b04852

De Smedt, I., Yu, H., Richter, A., Beirle, S., Eskes, H., Boersma, K. F., et al. (2017). *QA4ECV HCHO tropospheric column data from OMI*. Royal Belgian Institute for Space. Version 1.1 [Data set]. http://doi.org/10.18758/71021031

Duncan, B. N., Prados, A. I., Lamsol, L. N., Liu, Y., Streets, D. G., Gupta, P., et al. (2014). Satellite data of atmospheric pollution for U.S. air quality applications: Examples of applications, summary of data end-user resources, answers to FAQs, and common mistakes to avoid. *Atmospheric Environment*, *94*, 647–662. https://doi.org/10.1016/j.atmosenv.2014.05.061

Fan, Y., & van den Dool, H. (2008). A global monthly land surface air temperature analysis for 1948-present. *Journal of Geophysical Research*, *113*(D1). https://doi.org/10.1029/2007jd008470

Fletcher, K., & McMullan, K. (2016). *Sentinel 5 precursor: ESA's atmospheric chemistry and pollution-Monitoring Mission*. European Space Agency.

Fortunati, A., Barta, C., Brilli, F., Centritto, M., Zimmer, I., Schnitzler, J., & Loreto, F. (2008). Isoprene emission is not temperature-dependent during and after severe drought-stress: A physiological and biochemical analysis. *The Plant Journal*, *55*(4), 687–697. https://doi.org/10.1111/j.1365-313x.2008.03538.x

Fried, A., Barth, M. C., Bela, M., Weibring, P., Richter, D., Walega, J. et al. (2016). Convective transport of formaldehyde to the upper troposphere and lower stratosphere and associated scavenging in thunderstorms over the central United States during the 2012 DC3 study. *Journal of Geophysical Research Atmospheres*, *121*(12), 7430–7460. https://doi.org/10.1002/2015jd024477

Friedl, M., & Sulla-Menashe, D. (2019). MCD12Q1 MODIS/Terra+Aqua Land Cover Type Yearly L3 Global 500m SIN Grid V006. *NASA EOSDIS Land Processes DAAC*. Data set https://doi.org/10.5067/MODIS/MCD12Q1.006

Geron, C., Rasmussen, R., Arnts, R. R., & Guenther, A. (2000). A review and synthesis of monoterpene speciation from forests in the United States. *Atmospheric Environment*, *34*(11), 1761–1781. https://doi.org/10.1016/s1352-2310(99)00364-7

Guenther, A., Geron, C., Pierce, T., Lamb, B., Harley, P., & Fall, R. (2000). Natural emissions of non-methane volatile organic compounds, carbon monoxide, and oxides of nitrogen from North America. *Atmospheric Environment*, *34*(12–14), 2205–2230. https://doi.org/10.1016/s1352-2310(99)00465-3

Guenther, A., Hewitt, C. N., Erickson, D., Fall, R., Geron, C., Graedel, T., et al. (1995). A global model of natural volatile organic compound emission. *Journal of Geophysical Research*, *100*(D5), 8873–8892. https://doi.org/10.1029/94jd02950

Guenther, A., Zimmerman, P., & Wildermuth, M. (1994). Natural volatile organic compound emission rate estimates for U.S. woodland landscapes. *Atmospheric Environment*, *28*(6), 1197–1210. https://doi.org/10.1016/1352-2310(94)90297-6

Guenther, A., Zimmerman, P. R., Harley, P. C., Monson, R. K., & Fall, R. (1993). Isoprene and monoterpene emission rate variability: Model evaluations and sensitivity analyses. *Journal of Geophysical Research*, *98*(D7), 12609–12617. https://doi.org/10.1029/93jd00527

Hagerman, L. M., Aneja, V. P., & Lonneman, W. A. (1997). Characterization of non-methane hydrocarbons in the rural southeast United States. *Atmospheric Environment*, *31*(23), 4017–4038. https://doi.org/10.1016/s1352-2310(97)00223-9

Huber, D. E., Steiner, A. L., & Kort, E. A. (2020). Daily cropland soil NOx emissions identified by TROPOMI and SMAP. *Geophysical Research Letters*, *47*(22). https://doi.org/10.1029/2020gl089949

Hudman, R. C., Moore, N. E., Mebust, A. K., Martin, R. V., Russell, A. R., Valin, L. C., & Cohen, R. C. (2012). Steps toward a mechanistic model of global soil nitric oxide emissions: Implementation and space based-constraints. *Atmospheric Chemistry and Physics*, *12*, 7779–7795. https://doi.org/10.5194/acp-12-7779-2012

Hudman, R. C., Russell, A. R., Valin, L. C., & Cohen, R. C. (2010). Interannual variability in soil nitric oxide emissions over the United States as viewed from space. *Atmospheric Chemistry and Physics*, *10*(20), 13029–13053. https://doi.org/10.5194/acp-10-9943-2010

Jaeglé, L., Martin, R. V., Chance, K., Steinberger, L., Kurosu, T. P., Jacob, D. J., et al. (2004). Satellite mapping of rain-induced nitric oxide emissions from soils. *Journal of Geophysical Research*, *109*(D21), 2007–2023. https://doi.org/10.1029/2004jd004787

Jaeglé, L., Steinberger, L., Martin, R. V., & Chance, K. (2005). Global partitioning of NOx sources using satellite observations: Relative roles of fossil fuel combustion, biomass burning and soil emissions. *Faraday Discussions*, *130*, 407–423. https://doi.org/10.1039/b502128f

Jin, X., Fiore, A. M., Boersma, K. M., De Smedt, I., & Valin, L. (2020). Changes of summertime surface ozone-NOx-VOC chemistry over U.S. urban areas inferred from two decades of satellite and ground-based observations. *Environmental Science & Technology*. https://doi.org/10.1021/acs.est.9b07785

Keyantash, J. Ed., (2018). National Center for Atmospheric Research Staff *The climate data Guide: Standardized precipitation index (SPI)*. Retrieved from https://climatedataguide.ucar.edu/climate-data/standardized-precipitation-index-spi

Koppmann, R., Czapiewski, K. V., & Reid, J. S. (2005). A review of biomass burning emissions, part I: Gaseous emissions of carbon monoxide, methane, volatile organic compounds, and nitrogen containing compounds. *Atmospheric Chemistry and Physics*, *5*, 10455–10516. https://doi.org/10.5194/acpd-5-10455-2005

Lelieveld, J., Evans, J. S., Fnais, M., Giannadaki, D., & Pozzer, A. (2015). The contribution of outdoor air pollution sources to premature mortality on a global scale. *Nature*, *525*, 367–371. https://doi.org/10.1038/nature15371

Lerdau, M., & Keller, M. (1997). Controls on isoprene emission from trees in a subtropical dry forest. *Plant, Cell and Environment*, *20*(5), 569–578. https://doi.org/10.1111/j.1365-3040.1997.00075.x

Levelt, P. F., van den Oord, G. H. J., Dobber, M. R., Malkki, A., Visser, H., de Vries, J., et al. (2006). The ozone monitoring instrument. *IEEE Transactions on Geoscience and Remote Sensing*, *44*(5), 1093–1101. https://doi.org/10.1109/tgrs.2006.872333

Logan, J. A. (1983). Nitrogen oxides in the troposphere: Global and regional budgets. *Journal of Geophysical Research*, *88*(C15), 10785–10807. https://doi.org/10.1029/jc088ic15p10785

Malley, C. S., Henze, D. K., Kuylenstierna, J. C., Vallack, H. W., Davila, Y., Anenberg, S. C., et al. (2017). Updated global estimates of respiratory mortality in adults ≥30years of age attributable to long-term ozone exposure. *Environmental Health Perspectives*, *125*(8), 087021-1–087021–9. https://doi.org/10.1289/ehp1390

Matthijsen, J., Suhre, K., Rosset, R., Eisele, F. L., Mauldin, R. L., III, & Tanner, D. J. (1998). Photodissociation and UV radiative transfer in a cloudy atmosphere: Modeling and measurements. *Journal of Geophysical Research*, *103*(D13), 16665–16676. https://doi.org/10.1029/97jd02989

McKee, T. B., Doesken, N. J., & Kleist, J. (1993). The relationship of drought frequency and duration to time scales. Paper presented at *Proceedings of the 8th Conference on Applied Climatology* (Vol. *17*, pp. 179–183).

Oikawa, P. Y., Ge, C., Wang, J., Eberwein, J. R., Liang, L. L., Allsman, L. A., et al. (2015). Unusually high soil nitrogen oxide emissions influence air quality in a high-temperature agricultural region. *Nature Communications*, *6*. https://doi.org/10.1038/ncomms9753

Ormeño, E., Mévy, J. P., Vila, B., Bousquet-Mélou, A., Greff, S., Bonin, G., & Fernandez, C. (2007). Water deficit stress induces different monoterpene and sesquiterpene emission changes in Mediterranean species. Relationship between terpene emissions and plant water potential. *Chemosphere*, *67*(2), 267–284. https://doi.org/10.1016/j.chemosphere.2006.10.029

Pegoraro, E., Rey, A., Baron-Gafford, G., Monson, R., Malhi, Y., & Murthy, R. (2005). The interacting effects of elevated atmospheric CO_2 concentration, drought and leaf-to-air vapor pressure deficit on ecosystem isoprene fluxes. *Oecologia*, *146*(1), 120–129. https://doi.org/10.1007/s00442-005-0166-5

Pfister, G. G., Emmons, L. K., Hess, P. G., Lamarque, J.-F., Orlando, J. J., Walters, S., et al. (2008). Contribution of isoprene to chemical budgets: A model tracer study with the NCAR CTM MOZART-4. *Journal of Geophysical Research*, *113*(D5). https://doi.org/10.1029/2007jd008948

Potosnak, M. J., LeStourgeon, L., Pallardy, S. G., Hosman, K. P., Gu, L., Karl, T., et al. (2014). Observed and modeled ecosystem isoprene fluxes from an oak-dominated temperate forest and the influence of drought stress. *Atmospheric Environment*, *84*, 314–322. https://doi.org/10.1016/j.atmosenv.2013.11.055

Price, C. (1993). Global surface temperatures and the atmospheric electrical circuit. *Geophysical Research Letters*, *20*(13), 1363–1366. https://doi.org/10.1029/93gl01774

Price, C. (2009). Will a drier climate result in more lightning? *Atmospheric Research*, *91*(2–4), 479–484. https://doi.org/10.1016/j.atmosres.2008.05.016

Purves, D. W., Caspersen, J. P., Moorcroft, P. R., Hurtt, G. C., & Pacala, S. W. (2004). Human-induced changes in US biogenic volatile organic compound emissions: Evidence from long-term forest inventory data. *Global Change Biology*, *10*, 1737–1755. https://doi.org/10.1111/j.1365-2486.2004.00844.x

Sillman, S., Logan, J. A., & Wofsy, S. C. (1990). The sensitivity of ozone to nitrogen oxides and hydrocarbons in regional ozone episodes. *Journal of Geophysical Research*, *95*(D2), 1837–1851. https://doi.org/10.1029/jd095id02p01837

Sillman, S., & Samson, P. J. (1995). Impact of temperature on oxidant photochemistry in urban, polluted rural and remote environments. *Journal of Geophysical Research*, *100*(D6), 11497–11508. https://doi.org/10.1029/94jd02146

Singh, H. B., Cai, C., Kaduwela, A., Weinheimer, A., & Wisthaler, A. (2012). Interactions of fire emissions and urban pollution over California: Ozone formation and air quality simulations. *Atmospheric Environment*, *56*, 45–51. https://doi.org/10.1016/j.atmosenv.2012.03.046

Stocker, D. W., Stedman, D. H., Zeller, K. F., Massman, W. J., & Fox, D. G. (1993). Fluxes of nitrogen oxides and ozone measured by Eddy correlation over a shortgrass prairie. *Journal of Geophysical Research*, *98*(D7), 12619–12630. https://doi.org/10.1029/93jd00871

Strahler, A., Muchoney, D., Borak, J., Friedl, M., Gopal, S., Lambin, E., & Moody, A. (1999). *MODIS land cover product Algorithm Theoretical Basis Document (ATBD) version 5.0 MODIS land cover and land-cover change*. Boston University. Retrieved from https://modis.gsfc.nasa.gov/data/atbd/atbd_mod12.pdf

Tawfik, A. B., Stöckli, R., Goldstein, A., Pressley, S., & Steiner, A. L. (2012). Quantifying the contribution of environmental factors to isoprene flux interannual variability. *Atmospheric Environment*, *54*, 216–224. https://doi.org/10.1016/j.atmosenv.2012.02.018

Tost, H., Jöckel, P., Kerkweg, A., Pozzer, A., Sander, R., & Lelieveld, J. (2007). Global cloud and precipitation chemistry and wet deposition: Tropospheric model simulations with ECHAM5/MESSy1. *Atmospheric Chemistry and Physics*, *7*, 2733–2757. https://doi.org/10.5194/acp-7-2733-2007

Turtola, S., Manninen, A.-M., Rikala, R., & Kainulainen, P. (2003). Drought stress alters the concentration of wood terpenoids in scots pine and Norway spruce seedlings. *Journal of Chemical Ecology*, *29*, 1981–1995. https://doi.org/10.1023/a:1025674116183

University of East Anglia Climatic Research Unit, Harris, I. C., & Jones, P. D. (2017). *CRU TS3.24.01: Climatic Research Unit (CRU) Time-Series (TS) version 3.24.01 of high-resolution gridded data of month-by-month variation in climate*. Centre for Environmental Data Analysis. (January 1901- December 2015) [Data set]. http://dx.doi.org/10.5285/3df7562727314bab963282e6a0284f24

University of East Anglia Climatic Research Unit, Harris, I. C., & Jones, P. D. (2020). *CRU TS4.03: Climatic Research Unit (CRU) Time-Series (TS) version 4.03 of high-resolution gridded data of month-by-month variation in climate*. Centre for Environmental Data Analysis. (January 1901- December 2018) [Data set]. http://dx.doi.org/10.5285/10d3e3640f004c578403419aac167d82

Valin, L. C., Fiore, A. M., Chance, K., & Gonzàlez Abad, G. (2016). The role of OH production in interpreting the variability of CH2O columns in the southeast U.S. *Journal of Geophysical Research Atmospheres*, *121*(1), 478–493. https://doi.org/10.1002/2015jd024012

Vicente-Serrano, S. M., Beguería, S., & López-Moreno, J. I. (2010). A Multi-scalar drought index sensitive to global warming: The Standardized Precipitation Evapotranspiration Index – SPEI. *Journal of Climate*, *23*(7), 1696–1718. https://doi.org/10.1175/2009jcli2909.1

Vicente-Serrano, S. M., Beguería, S., López-Moreno, J. I., Angulo, M., & El Kenawy, A. M. (2010). A new global 0.5° gridded dataset (1901–2006) of a multiscalar drought index: Comparison with current drought index datasets based on the Palmer Drought Severity Index. *Journal of Hydrometeorology*, *11*(4), 1033–1043. https://doi.org/10.1175/2010jhm1224.1

Vinken, G. C. M., Boersma, K. F., Maasakkers, J. D., Adon, M., & Martin, R. V. (2014). Worldwide biogenic soil NOx emissions inferred from OMI NO2 observations. *Atmospheric Chemistry and Physics*, *14*(18), 10363–10381. https://doi.org/10.5194/acp-14-10363-2014

Wang, Y., Xie, Y., Dong, W., Ming, Y., Wang, J., & Shen, L. (2017). Adverse effects of increasing drought on air quality via natural processes. *Atmospheric Chemistry and Physics*, *17*(20), 12827–12843. https://doi.org/10.5194/acp-17-12827-2017

Weng, H., Lin, J., Martin, R., Millet, D. B., Jaeglé, L., Ridley, D., et al. (2020). Global high-resolution emissions of soil NOx, sea salt aerosols, and biogenic volatile organic compounds. *Scientific Data*, *7*(148). https://doi.org/10.1038/s41597-020-0488-5

Williams, E. J., & Fehsenfeld, F. C. (1991). Measurement of soil nitrogen oxide emissions at three North American ecosystems. *Journal of Geophysical Research*, *96*(D1), 1033–1042. https://doi.org/10.1029/90jd01903

Williams, E. J., Parrish, D. D., Buhr, M. P., Fehsenfeld, F. C., & Fall, R. (1988). Measurement of soil NOx emissions in central Pennsylvania. *Journal of Geophysical Research*, *93*(D8), 9539–9546. https://doi.org/10.1029/jd093id08p09539

Yienger, J. J., & Levy, H., II, (1995). Empirical model of global soil-biogenic NO_X emissions. *JGR Atmospheres*, *100*(D6), 11447–11464. https://doi.org/10.1029/95jd00370

Zhang, W., & Wang, Y. (2016). Climate-driven ground-level ozone extreme in the fall over the Southeast United States. *Proceedings of the National Academy of Sciences*, *113*(36), 10025–10030. https://doi.org/10.1073/pnas.1602563113

Zheng, Y., Unger, N., Barkley, M. P., & Yue, X. (2015). Relationships between photosynthesis and formaldehyde as a probe of isoprene emission. *Atmospheric Chemistry and Physics*, *15*, 8559–8576. https://doi.org/10.5194/acp-15-8559-2015

Zheng, Y., Unger, N., Tadić, J. M., Seco, R., Guenther, A. B., Barkley, M. P., et al. (2017). Drought impacts on photosynthesis, isoprene emission and atmospheric formaldehyde in a mid-latitude forest. *Atmospheric Environment*, *167*, 190–201. https://doi.org/10.1016/j.atmosenv.2017.08.017

Zhu, L., Jacob, D. J., Kim, P. S., Fisher, J. A., Yu, K., Travis, K. R., et al. (2016). Observing atmospheric formaldehyde (HCHO) from space: Validation and intercomparison of six retrievals from four satellites (OMI, GOME2A, GOME2B, OMPS) with SEAC4RS aircraft observations over the southeast US. *Atmospheric Chemistry and Physics*, *16*, 13477–13490. https://doi.org/10.5194/acp-16-13477-2016

Zhu, L., Mickley, L. J., Jacob, D. J., Marais, E. A., Sheng, J., Hu, L., et al. (2017). Long-term (2005-2014) trends in formaldehyde (HCHO) columns across North America as seen by the OMI satellite instrument: Evidence of changing emissions of volatile organic compounds. *Geophysical Research Letters*, *44*(13), 7079–7086. https://doi.org/10.1002/2017gl073859

Zoogman, P., Liu, X., Suleiman, R. X., Pennington, W. F., Flittner, D. E., Al-Saadi, J. A., et al. (2017). Tropospheric emissions: Monitoring of pollution (TEMPO). *Journal of Quantitative Spectroscopy and Radiative Transfer*, *186*, 17–39. https://doi.org/10.1016/j.jqsrt.2016.05.008

Zscheischler, J., Michalak, A. M., Schwalm, C., Mahecha, M. D., Huntzinger, D. N., Reichstein, M., et al. (2014). Impact of large-scale climate extremes on biospheric carbon fluxes: An intercomparison based on MsTMIP data. *Global Biogeochemical Cycles*, *28*(6), 585–600. https://doi.org/10.1002/2014gb004826